Carbon 158 (2020) 559–567

Contents lists available at ScienceDirect

Carbon

journal homepage: www.elsevier.com/locate/carbon

Tunable localized surface plasmon graphene metasurface for multiband superabsorption and terahertz sensing

M.S. Islam [a, b, *], J. Sultana [a], M. Biabanifard [c], Z. Vafapour [d], M.J. Nine [e], A. Dinovitser [a], C.M.B. Cordeiro [b, f], B.W.-H. Ng [a], D. Abbott [a]

[a] School of Electrical & Electronic Engineering, University of Adelaide, SA, 5005, Australia
[b] Institute of Photonics and Advanced Sensing, University of Adelaide, SA, 5005, Australia
[c] Advance Electromagnetic Laboratory, K. N. Toosi University of Technology, Tehran, 16315-1355, Iran
[d] Department of Electrical & Computer Engineering, Johns Hopkins University, Baltimore, 21218, Maryland, USA
[e] School of Chemical Engineering and Advanced Materials, University of Adelaide, SA, 5005, Australia
[f] Institute of Physics, University of Campinas, Campinas, 13083-859, Brazil

ARTICLE INFO

Article history:
Received 10 September 2019
Received in revised form
28 October 2019
Accepted 9 November 2019
Available online 18 November 2019

Keywords:
Graphene
Metasurface
Absorber
Terahertz sensor

ABSTRACT

We propose a plasmon induced tunable metasurface for multiband superabsorption and terahertz sensing. It consists of a graphene sheet that facilitates perfect absorption where the graphene pattern at the top layer creates an enhanced evanescent wave that facilitates the metasurface to work as a sensor. The modelling and numerical analysis are carried out using Finite Element Method (FEM) based software, CST microwave studio where a genetic algorithm (GA) is used to optimize the geometric parameters, and metasurface tunability is achieved via an external gate voltage on the graphene. By exploiting graphene's tunable properties we demonstrate a multiband superabsorption spectra having a maximum absorption of 99.7% in a frequency range of 0.1–2.0 THz that also maintain unique optical performance over a wide incidence angle. Further results show how the superabsorber can be used as a sensor, where the resonance frequency shifts with the refractive index of the surrounding environment.

1. Introduction

Plasmonic superabsorption (also known as perfect absorption) and wave trapping by means of plasmonic metasurfaces have attracted considerable attention due to promising new techniques for light manipulation, with potential applications in the field of energy harvesting, filtering, thermal imaging, electromagnetically induced transparency, and high performance sensing [1–5]. A promising pathway to take advantage of the above applications is to employ metasurfaces, offering a wide degree of freedom for tailoring the material's electromagnetic (EM) properties. Manipulation of an incident wave in a metasurface is followed by transmission or reflection propagation modes. For the transmission mode, several challenges, including transmission efficiency, obstruct its large scale deployment. The theoretical upper limit of the transmission efficiency of an ultra thin metasurface is about 25% [6]. Transmission efficiency can be increased by making the metasurface thin [7]. Compared to the transmission type metasurface, the metasurface designed to operate in reflection mode, can achieve an efficiency of close to 100%. This is because a metasurface can be made highly reflective, while also modulating the reflected wave by suitably tailoring the phase [8].

The excitation of plasmons within sub-wavelength structures on the metasurface leads to localization of electric and magnetic fields [9,10,12], creating strong light-matter interaction suitable for sensing [5,12,13]. Plasmons at the surface facilitate strong interaction with the surrounding environment [13], enabling the application of the superabsorber for sensing of dielectrics that have spectral signatures at terahertz frequencies [11,13].

While there have been a number of previous studies that have demonstrated absorption with terahertz metamaterials [15,17–21], these suffer low light-matter interaction with a low figure of merit. Moreover, proposed metamaterial devices not only exhibit extensive losses but also present numerous challenges to nanofabrication, requiring a large number of layers [22]. Previously, it has been shown that significant field trapping and enhancement

* Corresponding author. School of Electrical & Electronic Engineering, University of Adelaide, SA, 5005, Australia.
E-mail address: mdsaiful.islam@adelaide.edu.au (M.S. Islam).

https://doi.org/10.1016/j.carbon.2019.11.026
0008-6223/

can be obtained by exploiting the multilayer structure of metamaterials or metasurfaces forming a Fabry-Perot (F–P) cavity where absorption enhancement occurs due to increased light-matter interaction with multiple reflections inside the cavity [23]. Therefore, multilayered metamaterials have been proposed however those were able to achieve single [24] and triple [25] absorption band in the terahertz frequency range. Beside terahertz metamaterials and metasurfaces, various fiber optic [27,28] and planar [29–31] plasmonic sensors are also studied and investigated in the visible to infrared region, however, those sensors are suitable to detect bio-analytes that have a spectral fingerprint in the frequency of interests. In comparison with terahertz sensors [15,17–21,32], the microwave biosensor requires large area whereas the plasmonic sensors in the visible to infrared range [29–31,33] requires complicated fabrication process [34]. Moreover, many complex molecules have collective vibrational and rotational fingerprints in terahertz region, resulting in unique characteristic spectra [25,26]. Suitable terahertz sensors are of importance for capturing the terahertz 'fingerprint' of materials and complex molecules.

The metasurface perfect absorber based on the excitation of surface plasmon polaritons (SPPs) has the common problem of a single-band, which greatly limits its application especially for infrared detection, imaging, and sensing devices. The multi-band absorbers have greater tuneability than the single band absorbers. All multiband perfect absorbers are based on the combination of fundamental plasmon resonances of different sized periodic metallic/dielectric resonators. The strong interaction between the different resonators greatly limits the number of perfect absorption bands. Excitation of higher-order plasmon resonances is a promising way to design multi-band absorbers with over four absorbance bands.

Recently, graphene-based devices with multiple resonance excitations have been proposed that can be applied to enhance the light-matter interaction, increasing the possibility for multiband sensing. Multiple channels and multiplexing operations are highly required in systems including optical communication, absorbers, spectroscopy and sensors, and filters [36]. Recent studies show that multiband absorbers are essential for frequency selective detection that reduces environmental disturbance and enhances detection accuracy. Moreover, for the applications in terahertz thermal imaging, multiple-band absorbers, especially those that have more than four resonance peaks are in critical need of development [23,35].

Therefore, considering the efficiency of metasurface operational modes and application of multiple band absorbers, we propose a multilayer graphene metasurface that is able to trap the light strongly and enhance the surface plasmon effect. A gold mirror is used to reflect the incident terahertz waves, with tunable absorption in reflection mode and negligible transmission. We use high-resistive silicon between the gold and graphene sheet that also support the device. A dielectric Zeonex layer is used between graphene sheet and graphene pattern because of its suitable blend of properties in the terahertz band. Graphene sheet is used to increase the absorption whereas graphene pattern creates strong plasmons for enhanced sensing. To accelerate the design procedure we applied a genetic algorithm (GA) interface to CST to obtain the final design parameters.

2. Design, simulation and fabrication methodology

The unit cell of the proposed graphene metasurface is illustrated in Fig. 1 (a) where *Frequency domain solver* with *Floquet-port* boundary conditions are used to achieve the properties of the metasurface. The *Floquet-port*, where the unit cells are defined in the *x* and *y* directions and open space in *z*-direction, is used exclusively with planar-periodic structures. In the z-axis, perfectly matched layer (PML) is used to guarantee no scattering, leading to the accuracy of the results. Common examples are phased arrays and frequency selective surfaces which can be idealized as infinitely large. The analysis of the infinite structure is then accomplished by analyzing a unit cell. Linked boundaries most often form the sidewalls of a unit cell, but in addition, a boundary condition is required to account for the infinite space above. The *Floquet-port* is designed for this purpose. Boundaries that are adjacent to a *Floquet-port* must be linked boundaries. More detail on the *Floquet-port* boundary condition is given in Supplementary Material I. We select the *tetrahedral* mesh type having adaptive mesh refinement, the mesh subdivides the structure into a large number of tetrahedrons, which is required to achieve the desired simulation accuracy. To ensure zero transmission, the gold dispersive medium with a thickness larger than the penetration depth of terahertz is used

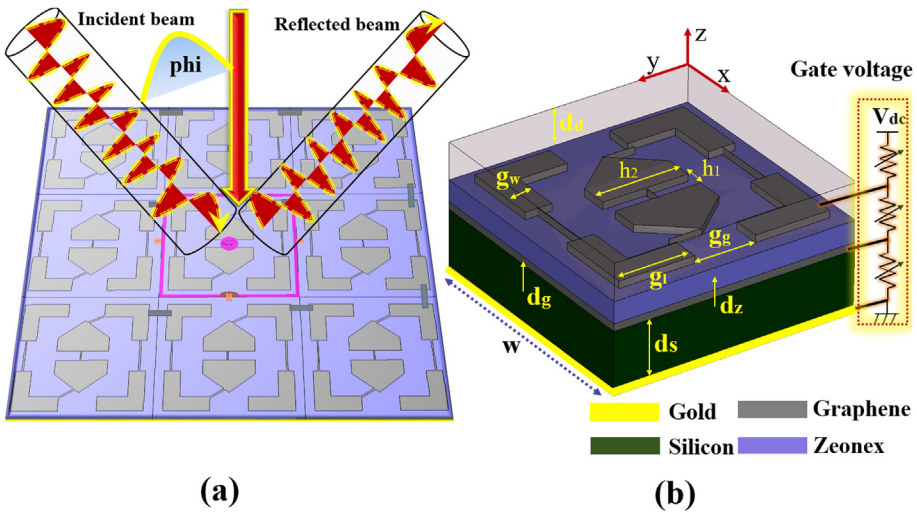

Fig. 1. (a) The proposed metasurface showing the incident and reflected terahertz beam, (b) the unit cell showing dimensions of different geometrical parameters including the electrical connection among the layers, the chronology of materials from the bottom layer is gold-silicon-graphene sheet-Zeonex-graphene pattern. (A colour version of this figure can be viewed online.)

[50]. The graphene sheet is used to enhance the absorption and the graphene pattern enhances plasmonic fields, which are beneficial for sensing applications.

The relative permittivity of gold is described by the Drude model [51],

$$\varepsilon(\omega) = \varepsilon_{\infty} - \frac{\omega_p^2}{\omega^2 + i\omega\gamma} \tag{1}$$

where, ε_{∞}, ω_p, and γ are the permittivity at infinite frequency, plasma frequency and collision frequency representing loss. These values for gold are 1.0, 1.38×10^{16} rad$\cdot$s^{-1} and 1.23×10^{13} s^{-1} respectively, and for silicon are 11.68, 4.94×10^{13} rad$\cdot$ s^{-1}, and 1.117×10^{13} s^{-1} respectively [51].

Another Drude-type semiconductor, silicon, is a dissipative element that supports the metasurface. Silicon can be regarded as a highly lossy material in the terahertz regime and can be easily processed using standard lithography technologies. The relative permittivity of silicon can be obtained following Eq. (1), where $\varepsilon_{\infty} = 11.7$. From the Hall effect analysis, the carrier concentration and electron mobility of the silicon wafer are measured to be 8.8×10^{16} cm^{-3} and 814.3 cm^{2}V^{-1}s^{-1} respectively. They correspond to $\omega_p = 4.94 \times 10^{13}$ rad$\cdot$s^{-1} and $\gamma = 1.117 \times 10^{13}$ s^{-1} which are used in the design [52,53].

In order to achieve optimal results in terahertz, we also select cyclo-olefin polymer (COP), Zeonex as another dielectric. The relative permittivity of Zeonex is 2.34 [37,38,40]. Zeonex is chosen due to its unique optical properties such as low absorption loss, high glass transition temperature, negligible material dispersion, insensitivity to humidity, can be readily injection molded, or extruded into film and sheet [39,40,49]. It has very low absorption loss in the terahertz region that makes it suitable for terahertz applications. Moreover, Zeonex is resistive to most acids and solvents. Therefore, it is a suitable candidate for the substrate of an absorber in the terahertz region [39,40].

Note that, graphene is considered as one of the key materials for the proposed device, upon which the absorption and other applications related to perfect absorption is totally dependent. The graphene is a single layer of sp^2 carbon atoms arranged in a honeycomb lattice and has recently triggered research activities worldwide due to its remarkable optical, mechanical, and chemical properties [41,42]. The graphene permittivity $\varepsilon_{G,t}$ can be expressed as [43–48],

$$\varepsilon_{G,t} = 1 + j\frac{\sigma(\omega)}{\varepsilon_0 \omega d_g} \tag{2}$$

here ω is the angular frequency, d_g is the graphene thickness, and ε_0 is the permittivity in vacuum.

The surface conductivity (σ) of graphene including both intraband (σ_{intra}) and interband (σ_{inter}) transitions are governed by the Kubo formula [43–47],

$$\sigma(\omega, \tau, \mu_c, T) = \sigma_{intra} + \sigma_{inter} \tag{3}$$

$$\sigma_{intra}(\omega, \tau, \mu_c, T) = -j\frac{e^2 k_B T}{\pi\hbar^2(\omega - j2\tau)}\left(\frac{\mu_c}{k_B T} + 2\ln\left(e^{-\mu_c/k_B T} + 1\right)\right) \tag{4}$$

$$\sigma_{inter}(\omega, \tau, \mu_c, T) = -j\frac{e^2}{4\pi\hbar}\ln\left(\frac{2\mu_c + (\omega - j2\tau)\hbar}{2\mu_c - (\omega - j2\tau)\hbar}\right) \tag{5}$$

where e is the electron charge, μ_c is the graphene chemical potential, τ is the scattering rate that is considered 0.1 ps and where the reason for choosing this value is described in Supplementary Material I, T is the temperature in Kelvin that is considered 300 K for this proposed device, k_B is the Boltzmann's constant, and $\hbar = \frac{h}{2\pi}$ is the reduced Planck's constant. In order to use graphene in the simulation, the permittivity is calculated using Eq. (2) and imported using the user defined dispersion list of CST. The same importing process is repeated in case of any graphene parameter changes. Note that, to support the electrical gating process, the graphene patterns are electrically connected via thin 0.1 μm graphene-stripes [56]. More detail of the design procedure is discussed in Supplementary Material I.

In order to manufacture the proposed device, the following steps can be followed. Firstly, high-resistivity 98.28 μm thick silicon with gold coating on one side and graphene sheet on the other, can be deposited by chemical vapor deposition (CVD). The CVD grown graphene can also be transferred to the silicon substrate [16]. The thin 5.79 μm Zeonex layer can then be deposited by spin coating and cured at vacuum oven. The top graphene pattern can then be achieved using a standard lithography process [17].

2.1. Parameter optimization-genetic algorithm

The optimization of the proposed device parameters including the thickness of silicon and Zeonex, as well as the dimensions of the top graphene patterns, are carried out using the iterative genetic algorithm (GA) method with built-in optimization tools available in CST Microwave studio. Using GA, it is possible to find the optimized design parameters to achieve a certain goal. It generates points into parameter space and then refines them through multiple generations, with random parameter mutation. The set goal for our optimization was to achieve maximum reflection (S_{11}) within the frequency range 0.1–2.0 THz. In the GA, the population size was set to 4×8, maximum 30 iterations, a mutation rate of 60% with an anchor value of 10%. The optimized values obtained using GA are $d_s = 98.28$ μm, $d_z = 5.79$ μm, $w = 67.58$ μm, $g_w = 7.44$ μm, $g_g = 17.06$ μm, $g_l = 21$ μm, $h_1 = 5$ μm, $h_2 = 15.62$ μm, all the parameters are defined in Fig. 1b. We also place a dielectric layer in contact with the patterned graphene, with a thickness defined as d_d. Note that the graphene chemical potential and scattering rate are optimized manually with characteristics illustrated in Sec. III and Supplementary Material I.

2.2. Transmission line theory and equivalent circuit modelling of the proposed device

When the incident wave is perpendicular to the surface, the absorption A is obtained from the S-parameters by the formula

$$A = 1 - \left|S_{21}(\omega)\right|^2 - \left|S_{11}(\omega)\right|^2 \tag{6}$$

where S_{11} and S_{21} are considered as reflection and transmission coefficients respectively. Note that the silicon has a high refractive index, with gold thickness larger than the terahertz skin depth, there is negligible transmission through the structure with the transmission coefficient is equal to zero, $|S_{21}(\omega)| = 0$. Therefore, the simplified form to calculate the absorption for the proposed device is

$$A = 1 - \left|S_{11}(\omega)\right|^2. \tag{7}$$

We apply transmission line theory with the equivalent circuit model (ECM) for the proposed superabsorber, as shown in Fig. 2a. In the ECM, the bottom gold layer can be considered as a short transmission line, with the impedance of silicon, Zeonex and air

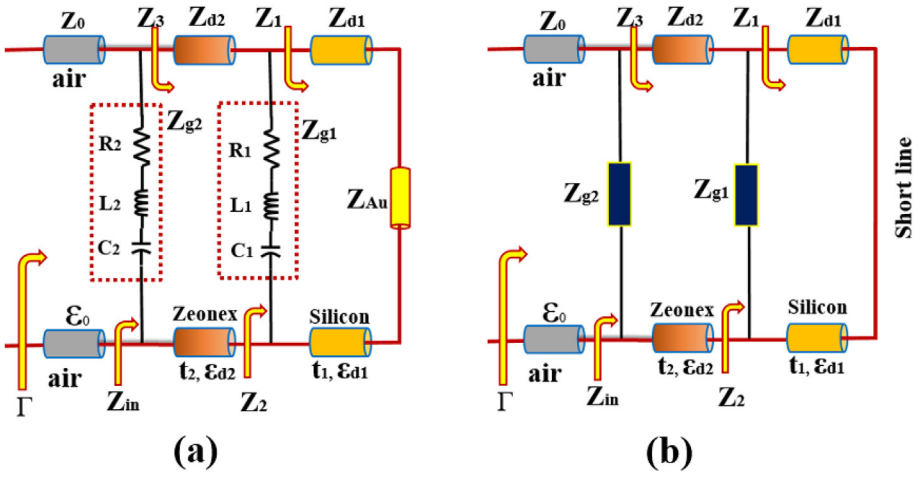

Fig. 2. (a) Equivalent circuit model for the graphene based tunable superabsorber; (b) simplified model. (A colour version of this figure can be viewed online.)

defined by Z_{d1}, Z_{d2} and Z_0. The impedance of metallic gold is denoted by Z_{Au} which is a short circuit in the simplified model of the ECM, as illustrated in Fig. 2b. The graphene sheet and graphene pattern is modeled by an RLC circuit network denoted by Z_{g1} and Z_{g2} in the ECM. The resistance R and the inductance L are a property of graphene, whereas the capacitance C is created by the gap between the graphene pattern and the graphene gate. In the ECM, the transmission channel corresponding to free space is denoted as Z_0, with the input surface impedance of the ECM shown as follows,

$$Z_1 = jZ_{d_s} \cdot \tan(\beta_d d_s) \tag{8}$$

$$Z_2 = \frac{Z_1 \cdot Z_{g_1}}{Z_1 + Z_{g_1}} \tag{9}$$

$$Z_3 = Z_{d_z} \frac{Z_2 + jZ_{d_z} \cdot \tan(\beta_d d_z)}{Z_{d_z} + jZ_2 \cdot \tan(\beta_d d_z)} \tag{10}$$

$$Z_{in} = \frac{Z_3 \cdot Z_{g_2}}{Z_3 + Z_{g_2}} \tag{11}$$

where $Z_{ds} = \frac{Z_0(120 \cdot \pi)}{\varepsilon_{ds}}$ is the impedance of silicon; $Z_{dz} = \frac{Z_0}{\varepsilon_{dz}}$ is the impedance of the Zeonex and β_d is the propagation constant of the propagating terahertz waves in the dielectric substances. Based on the effective medium theory the imaginary part of impedance must be equal to zero at the resonant point [54]. Therefore the corresponding reflection efficiency τ can be expressed as

$$\tau = S_{11} = \frac{\mathrm{Re}(Z_{in}) - Z_0}{\mathrm{Re}(Z_{in}) + Z_0}. \tag{12}$$

Note that, the dielectric permittivities of silicon, Zeonex and air are defined as ε_{ds}, ε_{dz} and ε_0 where d_s and d_z represent the silicon and Zeonex thickness.

3. Results and discussion

At normal incidence angle, the characteristics of reflection (R), transmission (T), and absorption (A) of the proposed metasurface is illustrated in Fig. 3 which shows a negligible transmission, highly efficient reflection and five bands of perfect absorption peaking at 99.7%, within a frequency range of 0.1–2.0 THz. The optimum parameters obtained using genetic algorithm (GA) are used, together with a graphene at a chemical potential of $\mu_c = 0.2$ eV. A graphene

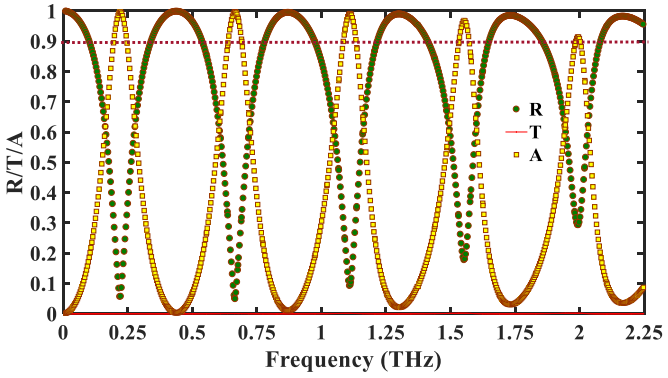

Fig. 3. The reflection (R), transmission (T), and absorption (A) characteristics of the proposed metasurface at optimized design parameters having $\mu_c = 0.2$ eV and at a normal incidence angle. (A colour version of this figure can be viewed online.)

thickness of 1 nm, equivalent to a tri-layer, was selected such that the appropriate mesh size resulted in a reasonably short simulation time [14]. Note that the metasurface is polarization insensitive as it shows similar optical characteristics at both transverse electric (TE) and transverse magnetic (TM) mode. Therefore for further simulation and characterization, we consider the TE polarization mode, further details about polarization are described in Supplementary Material I.

In later subsections of this manuscript, we discuss the physics of multiband absorption, the effect of graphene chemical potential, the effect of changing the incidence angle and performance of the metasurface at fabrication tolerances.

3.1. Mechanism of plasmon enhancement and multiband superabsorption

To explore the science behind multiband superabsorption, we show different mode fields including E-field, H-field, electric energy density, magnetic energy density, power flow and power flow density in Fig. 4a and Fig. 4b. It is found that different edges of graphene pattern excites at different frequencies, causing multiband resonance peaks. The excitation of the first plasmonic mode occurs when the frequency of the incoming photons matches with the first localized mode of the graphene pattern. Thus some photons are absorbed, and the others are reflected or transmitted through the graphene pattern. Transmitted photons are reflected

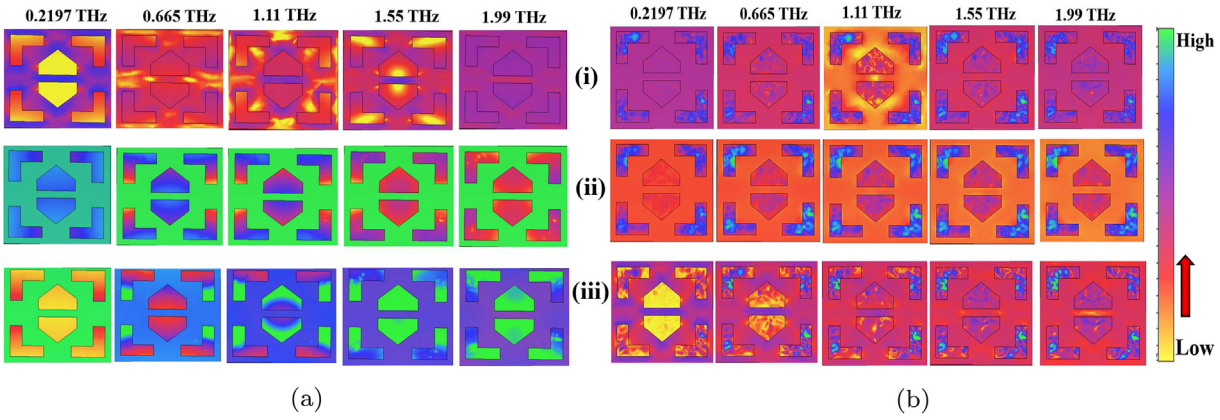

Fig. 4. (a), (i) E-field, (ii) electrical energy density, and (iii) power flow density; (b), (i) H-field, (ii) magnetic energy density, and (iii) power flow of the proposed device at optimized design parameters at resonance frequencies of 0.2197, 0.665, 1.11, 1.55 and 1.99 THz. (A colour version of this figure can be viewed online.)

back by the second graphene layer or eventually from the Au reflector, and some of them come out of the structure with a phase difference of $2\beta sd = \pi$, where d is the total distance travelled by the wave. This process is repeated multiple times, and these partial reflections destructively interfere with each other, leading to zero overall reflection. On the other hand, the transmission channel is closed by the Au reflector; thus, the incoming wave is completely trapped, and is finally absorbed in the structure.

The number of absorption bands of the proposed metasurface is dependent on the top graphene pattern and geometrical dimensions of Zeonex and silicon. These phenomena can be verified from Fig. 5a where a performance study with and without graphene sheet is shown. It can be seen that the resonance frequencies remain the same without the graphene sheet, therefore the graphene sheet does not have any effect on the number of absorption bands but have a strong affect in enhancing plasmons at the top graphene pattern. One way to have multi-band absorption is to design a unit cell that have Fabry-perot components with multiple resonating elements. The edges are then place where the plasmons can be excited with enhanced intensity. The intensity of fields at different resonance frequencies is shown in Fig. 4 where it can be seen that the surface plasmons are excited in different patterns at different frequencies and thus the metasurface acts as a multiband absorber. The phenomena of multiband absorption can also be explored from the Supplementary Material II. Note that, a possible way of converting the proposed multiband absorber to a broadband absorber would require to pattern both the graphene layer and tune the other geometrical properties.

The frequencies where high absorption is observed depends on the polymer dimensions. In order to exploit this effect, we increased the overall dimension by 20% while the top graphene pattern dimensions were kept the same. The obtained result is shown in Fig. 5b, where we see that as the dimension of the metasurface increases the resonance frequencies shift towards lower frequencies. Therefore, the operating frequency is totally dependent on the metasurface dimension, which can be chosen by design. Note that the separation between absorption peaks is regular, this is due to the structural symmetry and interference in the vertical cavity.

3.2. Dynamically tunable property enabled by graphene

The optical properties of graphene are highly dependent on its Fermi energy, which is considered as the origin of dynamic tunability of the proposed device. To realize tunability, we add an external bias voltage, as shown in Fig. 1, to modulate the chemical potential of graphene as described by the following equation [55],

$$\mu_c = \hbar v_f \sqrt{\frac{\pi \varepsilon_0 \varepsilon_{dz} \vee_g}{e d_z}} \tag{13}$$

where μ_c is the chemical potential of graphene, $\hbar$ is the Planck's

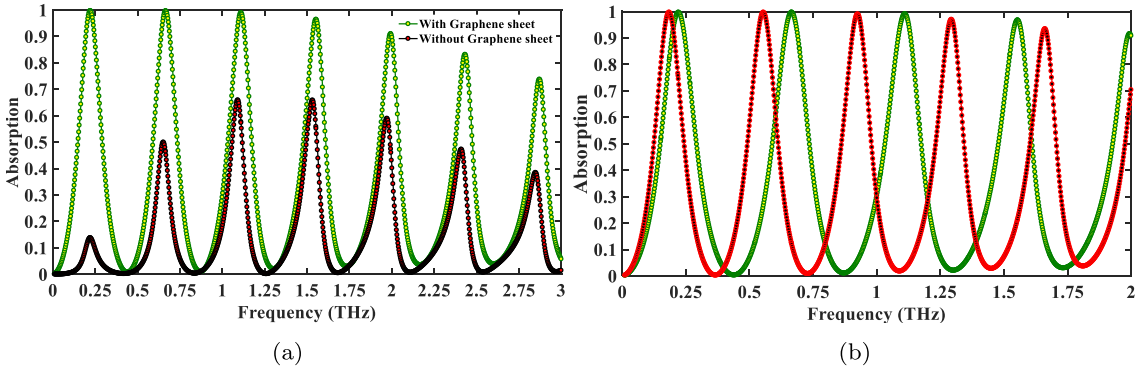

Fig. 5. (a) Effect of graphene sheet in between silicon and Zeonex on the overall performance of the metasurface, and (b) Dependence of resonance peaks on the overall dimension of the metasurface, the green line indicates the performance of the metasurface at an optimized dimension while the red line indicates the performance at 20% increased from its optimum dimension. (A colour version of this figure can be viewed online.)

constant, $v_f = 10^6$ m/s is the Fermi velocity, ε_0 and ε_r are the relative permittivity of vacuum and dielectric spacer respectively, e is the electron charge, $\vee_g$ is the external bias voltage, and d_z is the thickness of dielectric spacer between graphene sheet and graphene pattern.

In order to exploit the dynamic tunability property of the superabsorber, the chemical potential of graphene is varied from 0.01 to 1 eV. The characteristics is shown in Fig. 6a where it is observed that at $\mu_c = 0.01$ eV the metasurface does not act as a superabsorber because the absorption peaks do not reach high values (above 60%). However, as μ_c increases the amplitude of signal reflection decreases, therefore according to Eq. (7) the absorption also increases. It is found that for $\mu_c = 0.2$ eV, five-band superabsorption can be obtained having a maximum absorption of 99.7% within the frequency range of 0.1–2 THz. It is important to note we are defining superabsorption when its value exceeds 90% as indicated by the horizontal dashed line in Fig. 3 and 6a. The multiple bands are due to the plasmon excitation of different graphene patterns at different frequencies. An eight-band superabsorber can be obtained for a 0.4 eV, shown in Fig. 6b, causing a resonance shift to higher frequencies. Therefore, increasing μ_c increases the absorption bands and shifts the resonance to higher frequencies. One can choose a suitable μ_c considering the desired application and operating frequency range. In our case, we choose 0.2 eV for further characterization of the proposed device.

3.3. Wide angle of incidence

We further characterize the angle dependent response of the proposed plasmonic superabsorber that is illustrated in Fig. 7. As clearly shown that the absorber can achieve similar absorption performance up to around an oblique incidence angle of 70° however there is a shifting trends of absorption peaks towards the higher frequencies. For a particular angle (0° for example) it is noticeable that the absorption intensity decreases with the increase of frequency and therefore we obtain superabsorption upto around 2.0 THz and then the absorption decreases. These particular characteristics of the absorber are totally dependent on the geometrical parameters such as thickness of silicon, as well as the optical properties of Zeonex and graphene. Note that at normal incidence angle the parameters of the proposed superabsorber are optimized to operate in the low terahertz range (upto around 2.0 THz). However, these parameters can be tuned as required by application, performance, as well as the desired frequency range.

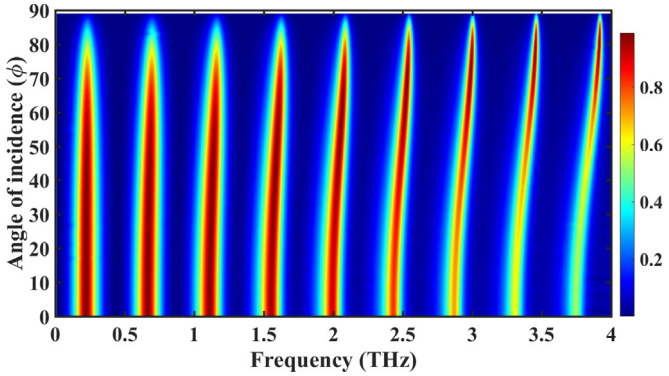

Fig. 7. Dependence of incident angle of the terahertz signal at optimized design conditions. The colourbar at the right side indicate the intensity of absorption, showing high intensity of absorption of around 2.0 THz with angle of incidence of around 70° which means the proposed absorber shows similar optical characteristics of upto around 70° and 2.0 THz. (A colour version of this figure can be viewed online.)

3.4. Characterization of the proposed device considering fabrication tolerances

Fabrication tolerances and their effect on device performance were estimated by varying the dimensions of the metasurface. The results are shown in Fig. 8, illustrating the reflection and absorption performance for a ±10% variation of dimensions. We find slight changes in the reflection and absorption curves, but no significant

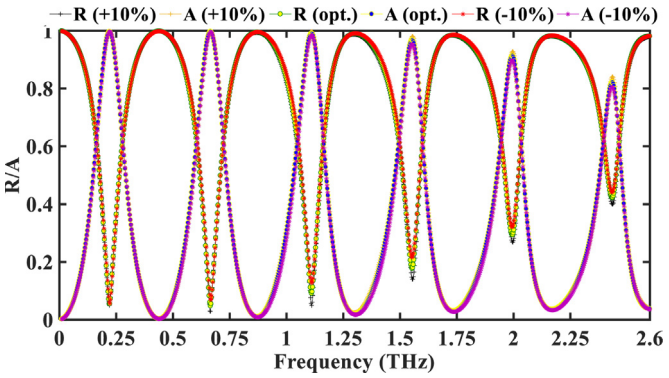

Fig. 8. Performance variation of the proposed superabsorber by varying the dimension of the metasurface to ±10%, under normal incidence angle and fixed graphene chemical potential of 0.2 eV. (A colour version of this figure can be viewed online.)

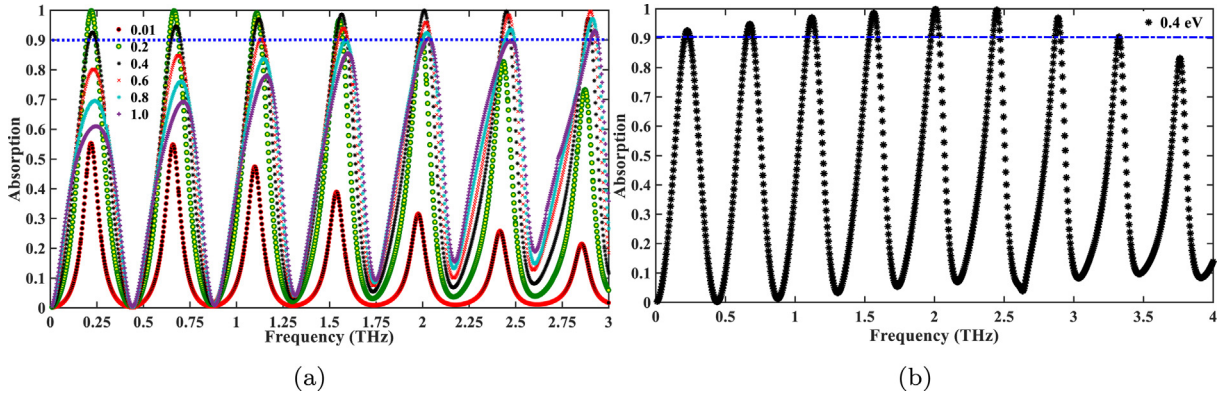

Fig. 6. (a) The tunability of the proposed metasurface at optimized design parameters by changing the graphene chemical potential at a normal incidence angle, and (b) Absorption at $\mu_c = 0.4$ eV to illustrate the effect of chemical potential on the overall performance of the absorber. (A colour version of this figure can be viewed online.)

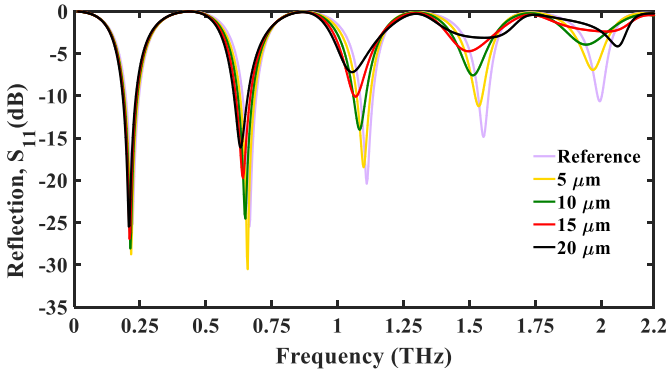

Fig. 9. Performance of the proposed device as a sensor at optimum design parameters, $\mu_c = 0.2$ eV and changing the dielectric layer thickness, d_d adjacent to the graphene pattern. (A colour version of this figure can be viewed online.)

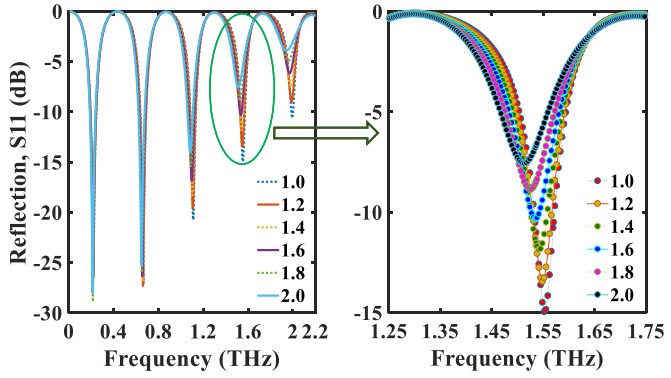

Fig. 10. Variation of resonance peak by changing the dielectric refractive indices adjacent to graphene pattern, by using optimum design parameters, $d_d = 10$ μm, and $\mu_c = 0.2$ eV. (A colour version of this figure can be viewed online.)

effect on the device performance.

4. Application to refractive index sensing

To simulate a sensing application, we applied a dielectric layer over the patterned graphene, and the characteristics of the sensor with different dielectric thickness, d_d, is illustrated in Fig. 9. We see that applying a dielectric in contact with the graphene pattern changes the reflection and resonance frequency, which is the desirable property enabling the application of the proposed device as a sensor. However, the d_d also has impact on the overall sensing performance, as observed in previous literature [57]. To verify this, we changed d_d and observed the performances. We found that increasing d_d increases the resonance shifts which also broadens the reflection peak. These result illustrates a broadened first full width at half maximum (FWHM), that in turn reduces the figure of merit (FOM), which is a function of FWHM (FOM = Sensitivity/FWHM) [58,59]. As the FWHM increases the FOM decreases, indicating overall performance reduction of the sensor. Comparing $d_d = 5$ and 10 μm, we see that 5 μm shows sharper resonance peaks however 10 μm shows improved sensing performance, albeit with a slight degradation of resonance quality factor. Further increase of d_d shows a larger FWHM. Therefore we found optimum sensitivity near $d_d = 10$ μm, and intend to carry out further characterization of the sensing properties of the device. Thus, considering d_d fixed at 10 μm we changed the refractive indices of the dielectric adjacent to graphene pattern, Fig. 10. We see that as the refractive index changes the resonance peak shifts, providing useable sensitivity.

The resonance frequency shift and sensing performance having different dielectric refractive index variation is shown in Fig. 11a where the FWHM is shown in Fig. 11b. These illustration indicate that as the dielectric refractive index increases the sensitivity also increases, due to the increasing concentration of dielectrics over the graphene surface. A linear approximation of the frequency shift is estimated using linear fitting that gives $R^2 = 0.9711$. The obtained value of R^2 indicate that the sensor have sufficient precision.

In terms of sensitivity, the limit of detection (LOD) is defined as the minimum level that can be detected with 99% fidelity. The LOD can be calculated by, LOD = 3ε/sensitivity, where ε denotes the output uncertainty or standard deviation. Considering a 1% standard deviation, the sensor achieves a maximum LOD of 4×10^{-4} [65, 66].

The characteristics of FWHM as shown in Fig. 11b indicate that as the dielectric refractive index and frequency increases the FWHM also increases, as the dielectric concentration and frequency increases, the resonance peak broadens.

A comparative analysis of the proposed device over the previously reported devices is carried out which is shown in Table 1. The comparison indicates that the proposed metasurface uses the localized plasmon mode that means the plasmons will be concentrated along some of the edges of the graphene pattern, which results in pentaband terahertz absorption, together with enhanced sensitivity.

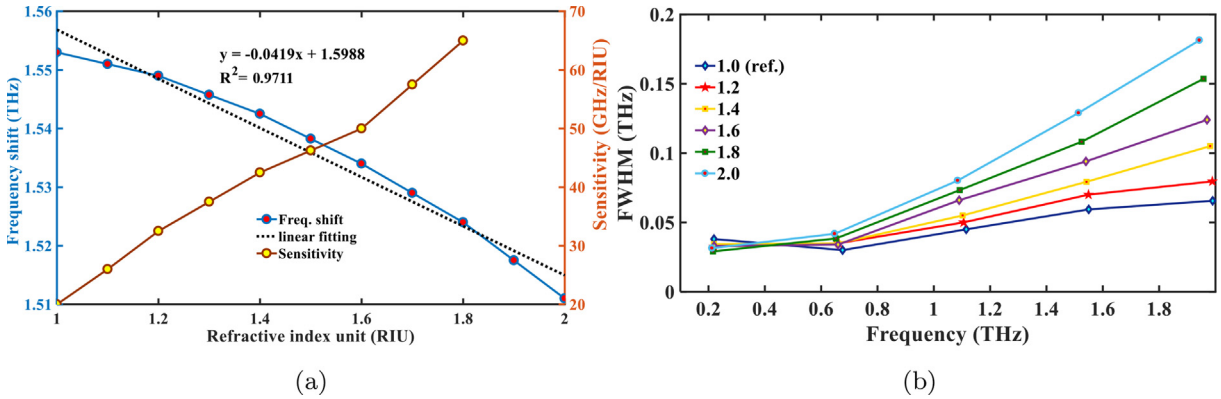

Fig. 11. (a) Frequency shift and sensitivity as a function of refractive index, The dotted line indicates an approximate linear fit. For the linear fit of the frequency shift curve we have $R^2 = 0.9711$; (b) achieved FWHM as a function of frequency. (A colour version of this figure can be viewed online.)

Table 1
Comparison of the proposed multiband device with prior reported devices.

Literature	Operating	Couple	Number of	Sensitivity
Refs.	band	mode	bands	
[60]	0.1–2 THz	plasmon	two	0.242 THz/RIU
[61]	0.5–0.9 THz	plasmon	one	23.5% RIU^{-1}
[62]	1.2–2.0 GHz	EIT-like	two	77.25 mm/RIU
[63]	0.1–100 THz	EIT-like	two	1200 nm/RIU
[64]	0.15–0.85 THz	plasmon	two	54.18 GHz/RIU
Proposed	0.1–2.25 THz	localized plasmon	five	66 GHz/RIU

5. Conclusion

We numerically demonstrate that a graphene based tunable metasurface can be used for multiband absorption and sensing. The field distributions in graphene pattern show the excited plasmons at different resonance frequencies that indicates the benefits of achieving multiband absorption. Varying the graphene chemical potential, the number of absorption bands can be varied. We show that at a chemical potential of 0.2 eV, the metasurface can achieve five absorption bands, which is promising for sensing applications. The metasurface has a maximum sensitivity of 66 GHz/ RIU, with a linearity of $R^2 = 0.9711$ and a considerable LOD. The metasurface can also illustrate similar optical performance over a wide acceptance angle of the incident terahertz beam that is also robust against fabrication tolerances. Owing to the above mentioned properties, the proposed metasurface is considered promising for multi-spectral applications of terahertz technology.

Funding statement

This work was supported by Australian Research Council (ARC) under grant DP170104984, also funded in part by the São Paulo Research Foundation (FAPESP) under grant 2018/10409.

Author contributions statement

M. S. Islam conceived the idea, design and simulation. All the authors analyzed the result. M. S. Islam wrote the manuscript which is then reviewed by all the authors. A. Dinovitser, Cristiano M. B. Cordeiro, B. W.-H. Ng and D. Abbott supervised the work. D. Abbott finally approves the manuscript for submission.

Declaration of competing interest

The authors declare that they have no known competing financial interests or personal relationships that could have appeared to influence the work reported in this paper.

Appendix A. Supplementary data

Supplementary data to this article can be found online at https://doi.org/10.1016/j.carbon.2019.11.026.

References

[1] J. Grant, I.J.H. McCrindle, D.R.S. Cumming, Multi-spectral materials: hybridisation of optical plasmonic filters, a mid infrared metamaterial absorber and a terahertz metamaterial absorber, Opt. Express 24 (4) (2016) 3451–3463.
[2] X. Yang, D. Zhang, S. Wu, Y. Yin, L. Li, K. Cao, K. Huang, Reconfigurable all-dielectric metasurface based on tunable chemical systems in aqueous solution, Sci. Rep. 7 (2017) 3190.
[3] H.K. Kim, D. Lee, S. Lim, A fluidically tunable metasurface absorber for flexible large-scale wireless ethanol sensor applications, Sensors 16 (8) (2016), 1246.
[4] Z. Liao, S. Liu, H.F. Ma, C. Li, B. Jin, T.J. Cui, Electromagnetically induced transparency metamaterial based on spoof localized surface plasmons at terahertz frequencies, Sci. Rep. 6 (2016) 27596.
[5] A. Keshavarz, Z. Vafapour, Sensing avian influenza viruses using terahertz metamaterial reflector, IEEE Sens. J. 19 (13) (2019) 5161–5166.
[6] F. Monticone, N.M. Estakhri, A. Alu, Full control of nanoscale optical transmission with a composite metascreen, Phys. Rev. Lett. 110 (2013), 203903.
[7] F. Qin, L. Ding, L. Zhang1, F. Monticone, C.C. Chum, J. Deng, S. Mei, Y. Li, J. Teng, M. Hong, S. Zhang, A. Alu, C.-W. Qiu, Hybrid bilayer plasmonic metasurface efciently manipulates visible light, Sci. Adv. 2 (1) (2016), e1501168.
[8] N. Yu, P. Genevet, M.A. Kats, F. Aieta, J.-P. Tetienne, F. Capasso, Z. Gaburro, Light propagation with phase discontinuities: generalized laws of reflection and refraction, Science 334 (6054) (2011) 333–337.
[9] P. Zheng, S. Kasani, N. Wu, "Converting plasmonic light scattering to confined light absorption and creating plexcitons by coupling a gold nano-pyramid array onto a silica–gold film, Nanoscale *Horiz.* 4 (2) (2019) 516–525.
[10] L. Wang, Q.-D. Chen, X.-W. Cao, R. Buividas, X. Wang, S. Juodkazis, H.-B. Sun, Plasmonic nano-printing: large-area nanoscale energy deposition for efficient surface texturing, Light Sci. Appl. 6 (2017), e17112.
[11] M. Beruete, I. Jáuregui-López, Optical fields in nanostructures: from sub-diffraction-limited optics to sensing and energy conversion, Adv. Optical Mater. 6 (2019) 1900721.
[12] X. Luo, D. Tsai, M. Gu, M. Hong, Terahertz sensing based on metasurfaces, Chem. Soc. Rev. 48 (8) (2019) 2458–2494.
[13] S. Zeng, K. Valiyaveedu, S. Jingzhi, S. Ting, Y. Chih-Kuan, C. Fen, Y. Dominique, B.P. Coquet, H.P. Ho, Andrei V. Kabashin Ken-Tye Yong, Graphene–gold metasurface architectures for ultrasensitive plasmonic biosensing, Adv. Mater. 27 (40) (2015) 6163–6169.
[14] Z. Liu, K. Aydin, Localized surface plasmons in nanostructured monolayer black phosphorus, Nano Lett. 66 (6) (2016) 3457–3462.
[15] X. Liu, C. Lan, B. Li, Q. Zhao, J. Zhou, Dual band metamaterial perfect absorber based on artificial dielectric molecules, Sci. Rep. 6 (2016) 28906.
[16] J. Kang, D. Shin, S. Bae, B.H. Hong, Graphene transfer: key for applications, Nanoscale 4 (18) (2012) 5527–5537.
[17] M.D. Astorino, R. Fastampa, F. Frezza, L. Maiolo, M. Marrani, M. Missori, M. Muzi, N. Tedeschi, A. Veroli, Polarization-maintaining reflection-mode THz time-domain spectroscopy of a polyimide based ultra-thin narrow-band metamaterial absorber, Sci. Rep. 8 (2018), 1985.
[18] B. Wu, Y. Hu, Y.T. Zhao, W.B. Lu, W. Zhang, Large angle beam steering THz antenna using active frequency selective surface based on hybrid graphene-gold structure, Opt. Express 26 (12) (2018) 15353–15361.
[19] C. Liu, L. Qi, X. Zhang, Broadband graphene-based metamaterial absorbers, AIP Adv. 8 (1) (2018), 015301.
[20] T.T. Nguyen, S. Lim, Bandwidth-enhanced and wide-angle-of-incidence metamaterial absorber using a hybrid unit cell, Sci. Rep. 7 (2017) 14814.
[21] J. Yang, Z. Zhu, J. Zhang, C. Guo, W. Xu, K. Liu, X. Yuan, S. Qin, Broadband terahertz absorber based on multi-band continuous plasmon resonances in geometrically gradient dielectric-loaded graphene plasmon structure, Sci. Rep. 8 (2018) 3239.
[22] C. Huang, W. Pan, X. Ma, X. Luo, Multi-spectral metasurface for dierent functional control of reflection waves, Sci. Rep. 6 (2016) 23291.
[23] H.T. Chen, Interference theory of metamaterial perfect absorbers, Opt. Express 20 (7) (2012) 7165–7172.
[24] X. He, Tunable terahertz graphene metamaterials, Carbon 82 (2015) 229–237.
[25] X. Chen, W. Fan, C. Song, Multiple plasmonic resonance excitations on graphene metamaterials for ultrasensitive terahertz sensing, Carbon 133 (2018) 416–422.
[26] Z.-P. Zheng, W.-H. Fan, H. Yan, Terahertz absorption spectra of benzene-1,2-diol, benzene-1,3-diol and benzene-1,4-diol, Chem. Phys. Lett. 525 (2012) 140–143.
[27] M.S. Islam, CristianoM.B. Cordeiro, J. Sultana, A.A. Rifat, R. Ahmed, S. Feng, A. Dinovitser, B.W.-H. Ng, D. Abbott, A Hi-Bi ultra-sensitive surface plasmon resonance fiber sensor, IEEE Access 7 (21) (2019) 79084–79094.
[28] M.S. Islam, J. Sultana, A.A. Rifat, M.S. Habib, A. Dinovitser, B.W.-H. Ng, D. Abbott, Localized surface plasmon resonance biosensor: an improved technique for SERS response intensification, Opt. Lett. 44 (5) (2019) 1134–1137.
[29] M. Abdelsalam, A.M. Mahmoud, M.A. Swillam, Polarization independent dielectric metasurface for infrared beam steering applications, Sci. Rep. 9 (2019), 10824.
[30] S. Gao, C.S. Park, S.-S. Lee, D.-Y. Choi, All-dielectric metasurfaces for simultaneously realizing polarization rotation and wavefront shaping of visible light, Nanoscale 11 (9) (2019) 4083–4090.
[31] L. Yang, D. Wu, Y. Liu, C. Liu, Z. Xu, H. Li, Z. Yu, L. Yu, H. Ye, High-efficiency all-dielectric transmission metasurface for linearly polarized light in the visible region, Photonics Res. 6 (6) (2018) 517–524.
[32] D. Christian, H.B. Peter, Frequency selective surfaces for high sensitivity terahertz sensing, Appl. Phys. Lett. 91 (2007) 184102.
[33] A.V. Kabashin, P. Evans, S. Pastkovsky, W. Hendren, G.A. Wurtz, R. Atkinson, R. Pollard, V.A. Podolskiy, A.V. Zayats, Plasmonic nanorod metamaterials for biosensing, Nat. Mater. 8 (2009) 867—871.

[34] T. Chen, S. Li, H. Sun, Metamaterials application in sensing, Sensors 12 (3) (2012) 2742–2765.
[35] B.-X. Wang, G.-Z. Wang, T. Sang, L.-L. Wang, Six-band terahertz metamaterial absorber based on the combination of multiple-order responses of metallic patches in a dual-layer stacked resonance structure, Sci. Rep. 7 (2017) 41373.
[36] J. Yao, Y. Chen, L. Ye, N. Liu, G. Cai, Q.H. Liu, Multiple resonant excitations of surface plasmons in a graphene stratified slab by Otto configuration and their independent tuning, Photonics Res. 5 (4) (2017) 377–384.
[37] J. Yang, Z. Zhu, J. Zhang, C. Guo, W. Xu, K. Liu, X. Yuan, S. Qin, Broadband terahertz absorber based on multi-band continuous plasmon resonances in geometrically gradient dielectric-loaded graphene plasmon structure, Sci. Rep. 8 (2018) 3239.
[38] A. Tuniz, B.T. Kuhlmey, Two-dimensional imaging in hyperbolic media-the role of field components and ordinary waves, Sci. Rep. 5 (2015) 17690.
[39] http://www.zeon.co.jp/business_e/enterprise/speplast/speplast1.html. *Accessdate:* 29*th April*, 2019.
[40] M.S. Islam, J. Sultana, C.M. B Cordeiro, A.L. S Cruz, A. Dinovitser, B.W.-H. Ng, D. Abbott, Broadband characterization of glass and polymer materials using THz-TDS, IRMMW-THz (2019) 1–2, https://doi.org/10.1109/IRMMW-THz.2019.8874013.
[41] K.S. Novoselov, A.K. Geim, S.V. Morozov, D. Jiang, Y. Zhang, S.V. Dubonos, I.V. Grigorieva, A.A. Firsov, Electric field effect in atomically thin carbon films, Science 306 (5596) (2004) 666–669.
[42] F. Bonaccorso, Z. Sun, T. Hasan, A.C. Ferrari, Graphene photonics and opto-electronics, Nat. Photonics 4 (5596) (2010) 611–622.
[43] B. Zhu, G. Ren, S. Zheng, Z. Lin, S. Jian, Nanoscale dielectric-graphene-dielectric tunable infrared waveguide with ultrahigh refractive indices, Opt. Express 21 (14) (2013) 17089–17096.
[44] Y. Liu, S. Jian, Tunable trapping and releasing light in graded graphene-silica metamaterial waveguide, Opt. Express 22 (20) (2014) 24312–24321.
[45] L. Yang, T. Hu, A. Shen, C. Pei, B. Yang, T. Dai, H. Yu, Y. Li, X. Jiang, J. Yang, Ultracompact optical modulator based on graphene-silica metamaterial, Opt. Lett. 39 (7) (2014) 1909–1912.
[46] J. Cheng, F. Fan, S. Chang, Recent progress on graphene-functionalized metasurfaces for tunable phase and polarization control, Nanomaterials 9 (3) (2019), 398.
[47] G.W. Hanson, Dyadic Green' functions and guided surface waves for a surface conductivity model of graphene, J. Appl. Phys. 103 (2008), 064302.
[48] E. Cao, X. Guo, L. Zhang, Y. Shi, W. Lin, X. Liu, Y. Fang, L. Zhou, Y. Sun, Y. Song, W. Liang, M. Sun, Electrooptical synergy on plasmon–exciton-codriven surface reduction reactions, Adv. Mater. Interfaces 4 (24) (2017), 1700869.
[49] P.D. Cunningham, N.N. Valdes, F.A. Vallejo, L.M. Hayden, B. Polishak, X.H. Zhou, J. Luo, K.Y.A. Jen, J.C. Williams, R.J. Twieg, Broadband terahertz characterization of the refractive index and absorption of some important polymeric and organic electro-optic materials, J. Appl. Phys. 109 (2011) 55–60.
[50] M. Biabanifard, M.S. Abrishamian, Ultra-wideband terahertz graphene absorber using circuit model, Appl. Phys. A 124 (12) (2018) 826.
[51] Z.H. Zhu, C.C. Guo, K. Liu, W.M. Ye, X.D. Yuan, B. Yang, T. Ma, Metallic nanofilm half-wave plate based on magnetic plasmon resonance, Opt. Lett. 37 (4) (2012) 698–700.
[52] M. Pu, Q. Feng, M. Wang, C. Hu, C. Huang, X. Ma, Z. Zhao, C. Wang, X. Luo, Ultrathin broadband nearly perfect absorber with symmetrical coherent illumination, Opt. Express 20 (3) (2012) 2246–2254.
[53] Y.Z. Cheng, W. Withayachumnankul, A. Upadhyay, D. Headland, Y. Nie, R.Z. Gong, M. Bhaskaran, S. Sriram, D. Abbott, Ultrabroadband plasmonic absorber for terahertz waves, Adv. Opt. Mater. 3 (3) (2015) 376–380.
[54] D.R. Smith, D.C. Vier, T. Koschny, C.M. Soukoulis, Electromagnetic parameter retrieval from inhomogeneous metamaterials, Adv. Opt. Mater. 71 (3) (2005).
[55] B. Liu, C. Tang, J. Chen, M. Zhu, M. Pei, X. Zhu, Electrically tunable fano resonance from the coupling between interband transition in monolayer graphene and magnetic dipole in metamaterials, Sci. Rep. 7 (2017) 17117.
[56] A. Fardoost, F.G. Vanani, A. Amirhosseini, R. Safian, Design of a multilayer graphene-based ultrawideband terahertz absorber, IEEE Trans. Nanotechnol. 16 (1) (2017) 68–74.
[57] X. Chen, W. Fan, Ultrasensitive terahertz metamaterial sensor based on spoof surface plasmon, Sci. Rep. 7 (2017), 2092.
[58] P. Offermans, M.C. Schaafsma, S.R.K. Rodriguez, Y. Zhang, M.C. Calama, S.H. Brongersma, J.G. Rivas, Universal scaling of the figure of merit of plasmonic sensors, ACS Nano 5 (6) (2011) 5151–5157.
[59] N. Muhammad, Z. Ouyang, Q. Liu, X. Tang, Z.-L. Deng, A.D. Khan, Sensitive label-free sensor with high figure of merit based on plasmonic metasurface with unit cell of double two-split nanorings, J. Mater. Sci. 54 (8) (2019) 6301–6309.
[60] X. He, S. Li, X. Yang, S. Shi, F. Wu, J. Jiang, High-sensitive dual-band sensor based on microsize circular ring complementary terahertz metamaterial, J. Electromagn. Waves Appl. 31 (1) (2017) 91–100.
[61] L. Cong, S. Tan, R. Yahiaoui, F. Yan, W. Zhang, R. Singh, Experimental demonstration of ultrasensitive sensing with terahertz metamaterial absorbers: a comparison with the metasurfaces, Appl. Phys. Lett. 106 (2015), 031107.
[62] F. Meng, Q. Wu, D. Erni, K. Wu, J. Lee, Polarization-independent metamaterial analog of electromagnetically induced transparency for a refractive-index-based sensor, IEEE Trans. Microw. Theory Tech. 60 (10) (2012) 3013–3022.
[63] C.-Y. Chen, I.-W. Un, N.-H. Tai, T.-J. Yen, Asymmetric coupling between subradiant and superradiant plasmonic resonances and its enhanced sensing performance, Opt. Express 17 (17) (2009) 15372–15380.
[64] R. Yahiaoui, S. Tan, L. Cong, R. Singh, F. Yan, W. Zhang, Multispectral terahertz sensing with highly flexible ultrathin metamaterial absorber, J. Appl. Phys. 8 (2015), 083103.
[65] R. Guider, D. Gandolfi, T. Chalyan, L. Pasquardini, A. Samusenko, C. Pederzolli, G. Pucker, L. Pavesi, Sensitivity and Limit of Detection of biosensors based on ring resonators, Sens. Bio-Sens. Res. 6 (2015) 99–102.
[66] J. Homola, Surface plasmon resonance sensors for detection of chemical and biological species, Chem. Rev. 108 (2) (2008) 462–493.